ACS OMEGA

http://pubs.acs.org/journal/acsodf

Article

Giant Dielectric Constant of Copper Nanowires/Amorphous SiO_2 Composite Thin Films for Supercapacitor Application

Anupam Maity, Subha Samanta, Shubham Roy, Debasish Biswas, and Dipankar Chakravorty*

Cite This: *ACS Omega* 2020, 5, 12421−12430

Read Online

ACCESS | Metrics & More | Article Recommendations

ABSTRACT: Transparent thin films comprising ultralong (within the range 52−387 μm) copper nanowires with diameter ∼7−9 nm encapsulated in amorphous silica have been successfully fabricated using an electrodeposition technique. The length and number density were controlled by electrodeposition time and concentration of precursor materials, respectively. Giant dielectric constant values (∼10^{10}) obtained from these systems were quantitatively explained as a function of the length of the nanowires on the basis of quantum mechanical theory derived by Rice and Bernasconi. These transparent thin films offer a specific capacitance value of 550 F/g with more than 73% cyclic stability over a period of 900 cycles. Our findings demonstrate a facile pathway to control and improve the properties of metal nanowire-based transparent materials for use in supercapacitor applications.

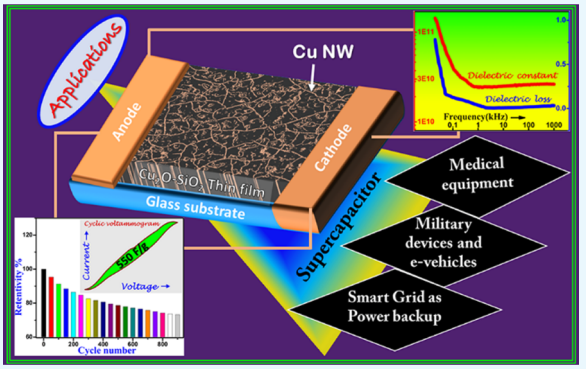

INTRODUCTION

The present trend of decrease in the use of traditional fossil fuels for reducing environmental hazards emanating from their indiscriminate use and also to be consistent with the trend of miniaturization of device having light weight have acted as catalysts to develop materials having large dielectric permittivity. With the increasing growth of renewable energy manufacturing units, the search for high-energy density capacitor without compromising on its optical transparency has been at its peak. Multifunctional nanoscale devices, including transparent conducting thin films, sensors, capacitors, and energy storage units, have been fabricated with nanowire composites or thin films.[1,2] Nanowire-based transparent thin film materials which can be used to create transparent electrodes for use in flat panel display, touch screen, and transparent supercapacitor have been of importance in recent times.[2] $BaTiO_3$ nanowires,[3] calcium copper titanate ($CaCu_3Ti_4O_{12}$) nanowires,[4] one-dimensional $BiFeO_3$ nanowires,[5] and polymer nanocomposites based on carbon nanotube/MnO_2 nanowires[6] thin film supercapacitors with the ruthenium oxide Lipon structure,[7] graphene-based supercapacitors,[8] porous nickel oxide thin films,[9,10] nanoporous $Ni(OH)_2$ thin films on graphite foam,[11] $CaCu_3Ti_4O_{12}$ (CCTO) with a dielectric constant value up to 10^5 at room temperature[12,13] have been studied to prepare high dielectric constant materials. The preparation methods for these materials involve complex reaction mechanisms with relatively long synthesis time and solid state reactions at high temperatures (∼1000 °C for 20 h).[14,15] Nanocomposites and thin films containing gold or silver nanowires have been studied for high-performance electrode or giant dielectric materials for use as supercapacitors.[16−18] As compared to silver, copper being more abundant and inexpensive has emerged as a good alternative. A series of copper-based nanowires with different morphologies have been synthesized by various methods.[19−21] In this context, an ultralong copper nanowire has been explored for the transparent electrode application.[2]

Large values of dielectric constant have been reported in suitably chosen composites of nanomaterials. For example, $BaTiO_3$ nanowires with an aspect ratio of 45.8 were reported to be having dielectric constant values of 44.3. The latter depended on the filler concentration and the aspect ratio of the nanowires.[3] Wet chemical synthesis followed by sintering at 1030 °C resulted in an increase of dielectric constant of $CaCu_3Ti_4O_{12}$ (CCTO) up to 10^5.[12] Such a high dielectric constant found in these materials was explained on the basis of the Maxwell−Wagner effect at the interface between the grains and grain boundaries.[22,23] Electrode polarization also plays a crucial role in determining the dielectric constant of a material.[24]

Received: March 17, 2020
Accepted: May 12, 2020
Published: May 21, 2020

https://dx.doi.org/10.1021/acsomega.0c01186
ACS Omega 2020, 5, 12421−12430

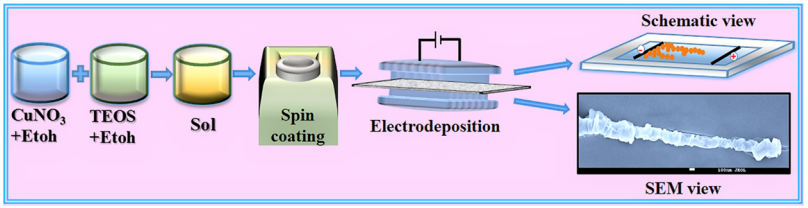

Figure 1. Structural schematic representation of silica-based transparent thin films containing copper nanowires.

Table 1. Summarized Data of Nanowire Lengths Associated with Dielectric Constant and Loss Values as a Function of Electrodeposition Time for All the Samples

sample	average number of nanowire heads within area of (50 × 50) nm^{-2} (n_d)	time of deposition (min)	average length of nanowires (μm)	dielectric constant at 1 MHz	dielectric loss at 1 MHz
thin film-1 (05 Cu_2O−95 SiO_2)	12	15	52	2.2×10^8	0.041
		30	53	2.3×10^8	0.043
		45	57	2.6×10^8	0.037
thin film-2 (15 Cu_2O−85 SiO_2)	25	05	183	5.6×10^9	0.019
		10	212	7.5×10^9	0.018
		15	387	2.5×10^{10}	0.011

Theoretical calculations by Kubo[25] opened a new direction by predicting that metallic nanoparticles would have discrete levels of electronic energy. Following these results, Gorkov and Eliashberg[26] showed that metallic nanoparticles will have large electronic polarizability at low temperatures. In this context, numerous experiments were performed but all showed negative results because of large depolarizing fields arising from the geometry of the nanoparticles.[27,28] Rice and Bernasconi proposed a model incorporating interrupted metallic nanowires which should exhibit a large dielectric constant but the latter would not be vitiated by a large depolarizing field.[17,18] Our findings on copper nanowire-based transparent thin films helped us to achieve the highest dielectric constant value ~10^{10} (at 1 MHz) reported to the best of our knowledge. Such a high value of dielectric constant was attributed to the quantum mechanical effect based on the Rice and Bernasconi model.[29]

Several studies regarding the dielectric effect on electrochemical properties of mixed transition metal oxides have been reported recently.[30] The predominant effect of grain and grain boundary of the crystallites on the electrochemical properties has been established.[30] CuS nanowire-based electrodes were successfully developed using a facile liquid−solid chemical oxidation process and an anion exchange reaction. These electrode materials exhibited areal capacitance of 378 mF/cm^2.[31] Nanoelectrodes comprising the CuS nanowire array on the copper foil were investigated for capacitive performance, and it showed a specific capacitance of 305 F/g at room temperature.[32] Cu_7S_4 nanowire coated on the carbon fiber fabric was studied as a binder-free electrode for a highly flexible solid state capacitor.[33] Comparative studies on capacitive performance of copper-based microstructures were investigated, and the nanowire $Cu(OH)_2$/Cu foil electrode offers the best supercapacitive performance with a specific capacitive value of 511.5 F/g.[34] Nanostructured materials comprising nanowires have attracted attention from scientific community for their exploitation as more efficient and stable electrodes for use in supercapacitor applications. Several studies have been carried out on nanowire-based materials having a high specific capacitance value and good cyclic stability for use in such applications.[5,16,35] Transparent electrodes based on polyaniline nanowires were reported as promising electrode materials with excellent capacitive performance exhibiting a specific capacitance value of 402 F/g.[36] Furthermore, capacitive behavior of NiO nanowire-based electrodes for the supercapacitor application was investigated depending on the morphology of the NiO nanostructures. The increased surface area of NiO nanowire helped to boost the capacitive performance.[37]

In this paper, we present a simple synthesis method of making well-aligned long copper nanowires at room temperature without the requirement of high annealing temperature. The thin films are transparent, and they exhibit a specific capacitance value of 550 F/g making them suitable for use in high-performance supercapacitor applications.

EXPERIMENTAL SECTION

The schematic for the synthesis procedure of silica-based transparent thin films containing copper nanowires is outlined, as shown in Figure 1. A facile sol−gel method was used to prepare our samples. All chemicals procured from Sigma-Aldrich with purity 99.99% were used without further purification. The target thin film compositions were 05 Cu_2O−95 SiO_2 (thin film-1) and 15 Cu_2O−85 SiO_2 (thin film-2). Tetraethyl orthosilicate (TEOS) and copper(II) nitrate trihydrate were used as silica and copper precursors, respectively. For the synthesis of the abovementioned compositions, calculated amount of TEOS was mixed with ethanol and stirred for 1 h in a beaker, and another solution was made by dissolving calculated proportion of copper nitrate in ethanol followed by stirring for 1 h in a separate beaker. These two solutions were then mixed and stirred for 7 h at room temperature to prepare the sol.

Commercially available glass slides with dimensions 1 × 1 cm^2 (supplied by Blue Star, India) were used as the substrate to prepare thin film samples. These glass slides were cleaned with acetone before thin film preparation. The as-prepared sol was spin coated (using Spin NXG-P1 supplied by Apex Equipment, India) with 1500 rpm for 2 min. The films thus prepared were kept in a desiccator at room temperature for 3 days.

For electrodeposition process, pure copper wires (supplied by KN Metal Trading Company, India) were used as electrodes and placed on the surface of the thin film containing

https://dx.doi.org/10.1021/acsomega.0c01186
ACS Omega 2020, 5, 12421−12430

Cu_2O-SiO_2 as the electrolyte (as shown in Figure 1). The separation between the electrodes was ∼6 mm with electrode lengths being ∼10 mm. Ultralong copper nanowires were formed when a dc voltage was applied across the electrodes. A constant dc voltage of 5 V magnitude was applied for different periods of time to grow nanowires of different lengths. The corresponding current−voltage ($I-V$) data were collected using the Keithley 2400 SourceMeter interfaced through LabVIEW program. The current through the samples increased with time indicating the formation of copper nanowires.[18] The lengths of the nanowires as a function of electrodeposition time is summarized in Table 1.

CHARACTERIZATIONS

The samples were characterized by X-ray diffraction patterns using a Bruker D8 XRD SWAX diffractometer with Cu Kα1 radiation operated at 40 kV and 40 mA. Atomic force microscopy (AFM) (Veeco model CP II) was used to find the thickness of the films. The noncontact tapping mode with a scanning rate of 0.5 Hz was used for data acquisition, and Proscan IP version 2.0 software was used for analysis and interpretation of data. The transparencies of the samples were measured using a UV−vis spectrophotometer (Agilent Technologies Cary 60 UV−vis). The surface morphology was studied using a field emission scanning electron microscope (JSM 7500F) operated at 15 kV. The microstructure of nanowires were further analyzed using a JEM 2010 transmission electron microscope (TEM) operated at 200 kV. Frequency-dependent dielectric constant and dissipation factor ($\tan\delta$) were measured using an LCR meter (Agilent E4980A). Cyclic voltammogram (CV) measurement was performed using a Neware BTS battery tester within the range of −1 to +1 V at the scan rates of 10, 30, 50, and 70 mV/s. The electrical measurements were carried out on the samples with the electrodes separated by a distance ∼6 mm and electrode lengths being ∼10 mm.

RESULTS AND DISCUSSION

Figure 2 shows the comparison of wide-angle X-ray diffraction patterns obtained from samples before electrodeposition and after electrodeposition of copper nanowires for thin film-1 and thin film-2. The peak positions from copper nanowire-based thin films correspond to the (111), (200), and (220) planes of copper as seen from the standard powder diffraction card of JCPDS (copper file no. 04-0836). A weak hump at around 22° reveals the presence of an insulating silica layer[38] which was further confirmed by TEM studies. The silica layer present in our sample is absolutely amorphous and does not possess any long-range periodicity. The amorphous nature is revealed by a weak hump at around 22°, which is in good agreement with JCPDS data (card no. 01-086-1561). Similar results were identified by other research groups as the signature of amorphous nature.[39] Also, the absence of any characteristic peaks for silica reconfirms that the sample did not crystallize and possessed no long-range periodicity.

The film thickness was measured using AFM (Veeco model CP II). For thickness measurement, the thin film was slashed with a sharp platinum blade, and the scanning was performed along this edge. A typical cross-sectional two-dimensional (2-D) image (inset) and the corresponding height profile of copper nanowire-based thin film-2 are shown in Figure 3a. Film thickness between the base of a scratch and the flat top

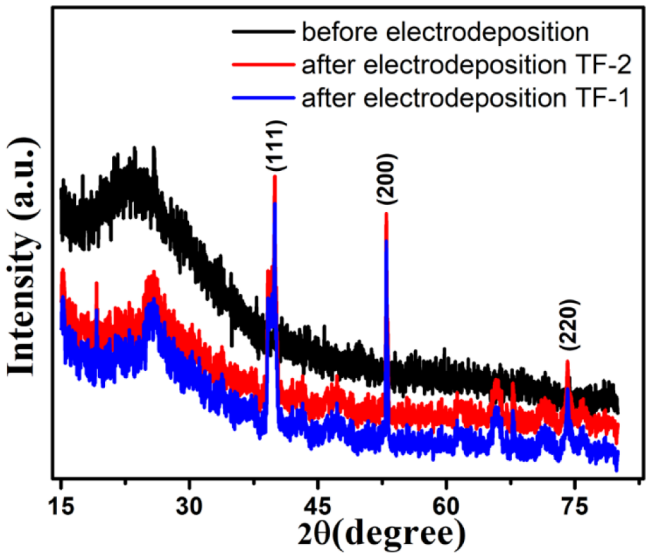

Figure 2. Comparison of wide-angle X-ray diffraction patterns obtained from samples before electrodeposition and after electrodeposition of copper nanowires for thin film-1 and thin film-2.

surface of the film was measured at several places, and the average thickness was estimated to be 380 nm. The corresponding three-dimensional (3-D) AFM image of the scanned edge is shown in Figure 3b; some of the small scrap that came out during the sample preparation process adhered to the surface and is clearly visible in the 3-D image.

Optical transparency of the copper nanowire-based thin films was measured using the UV−vis spectra over the optical wavelength range of 400−750 nm. The transmittance profile is shown in Figure 4. From figure, it is seen that these thin films exhibit a high transmittance of around 90% for thin film-1 and 60−80% for thin film-2. Such a high transparency makes these materials potentially suitable for use as a transparent supercapacitor.[1,36] The optical images of the thin films are shown in the inset of Figure 4.

Our facile synthesis procedure helped us to obtain well-aligned copper nanowires that is revealed in the TEM image of thin film-1, as shown in Figure 5. Inset of Figure 5a shows the disruption in nanowire arising because of a local heating effect which is further described in the subsequent section. Materials with high dielectric constant have been found to be limited for practical utility because of their high loss factors.[15,40] Our results revealed that giant dielectric constant values with low loss factors can be achieved with ease in the metallic nanowire system by following this preparation technique. A high-resolution transmission electron microscopy (HRTEM) image of thin film-1, as shown in Figure 5b, shows the silica layer and the copper nanowire with diameter ≈ 7−8 nm.

Figures 6a−c and 7a−c show the nanowire array density of the nanowire heads that were grown across an area of the sample perpendicular to the nanowire strands for thin film-1 and thin film-2. Figure 6a−c shows the variation of the nanowire array density for 15, 30, and 45 min of deposition time for thin film-1, and Figure 7a−c shows the variation of the nanowire array density for 5, 10, and 15 min of deposition time for thin film-2. These data indicate the high number density of uniformly distributed copper nanowires in these systems. It is important to note that the density of the nanowires grown in these systems was related to the concentration of the copper

https://dx.doi.org/10.1021/acsomega.0c01186
ACS Omega 2020, 5, 12421−12430

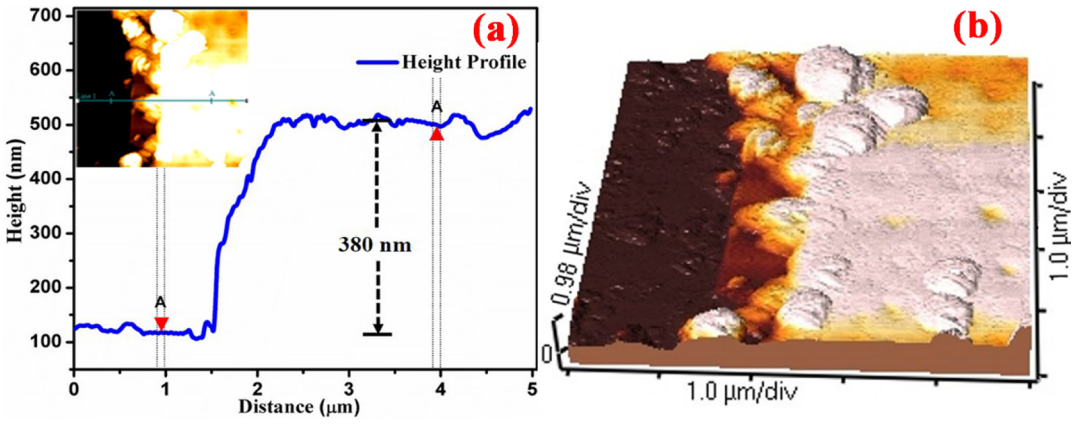

Figure 3. (a) Height profile of copper nanowire-based thin film. Inset shows cross-sectional 2-D image of the scanned edge. (b) 3-D AFM image obtained from inset of (a).

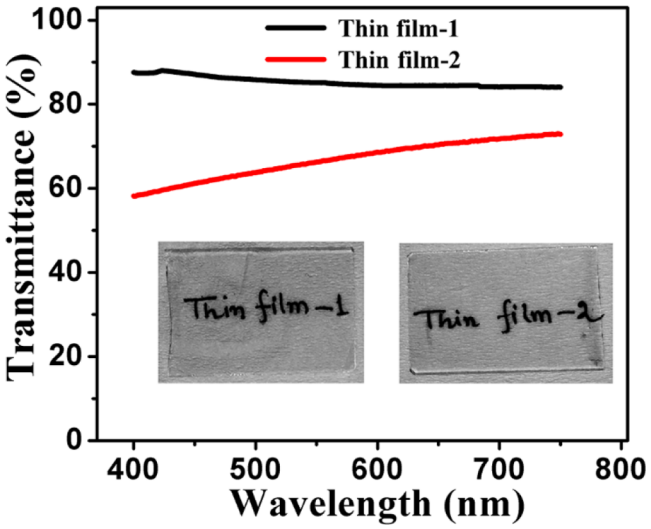

Figure 4. Transmittance profile of copper nanowire-based thin films. Inset shows optical images of the thin films.

ions in the starting material. The average nanowire array density data are summarized in Table 1 which have been used subsequently for the calculation of dielectric constant values from the theoretical model of Rice and Bernasconi. Insets of Figures 6a and 7a show the selected area electron diffraction (SAED) pattern and HRTEM image obtained from thin film-1 and thin film-2, respectively. The HRTEM image led to the identification of copper by measuring the *d*-spacing values of the lattice planes. The SAED (inset) confirmed the presence of Cu crystallites correlating it with the results obtained from HRTEM. The calculated *d*-spacing values can be indexed to the (111) planes which is in agreement with the reported data JCPDS (copper file no. 04-0836). It is to be noted that although the SAED pattern (Figure 6a) and HRTEM image (Figure 7a) were obtained from thin film-1 and thin film-2, respectively, we can safely conclude that both the Figures 6a and 7a indeed represent the images of copper nanowire heads, and additionally SAED pattern reveals the presence of the polycrystalline phase of copper in these systems.

The ultralong copper nanowires were clearly visible from the scanning electron microscopy (SEM) images, as shown in Figures 6d–f and 7d–f, for thin film-1 and thin film-2. The time of electrodeposition varied which resulted in the formation of copper nanowires with various lengths. The controlled growth of copper nanowires showing the variation of the length for thin film-1 and thin film-2 were evident from SEM images, as shown in Figures 6d–f and 7d–f. Figure 6d–f shows the variation of the nanowire length for 15, 30, and 45 min of deposition time for thin film-1, and Figure 7d–f shows the variation of the nanowire length for 5, 10, and 15 min of deposition time for thin film-2. The maximum nanowire length of ∼387 μm was obtained for thin film-2 after 15 min of deposition time. An SEM–energy-dispersive system (EDS) scanning microscope integrated with automated digital particle counting and imaging facility was employed to obtain

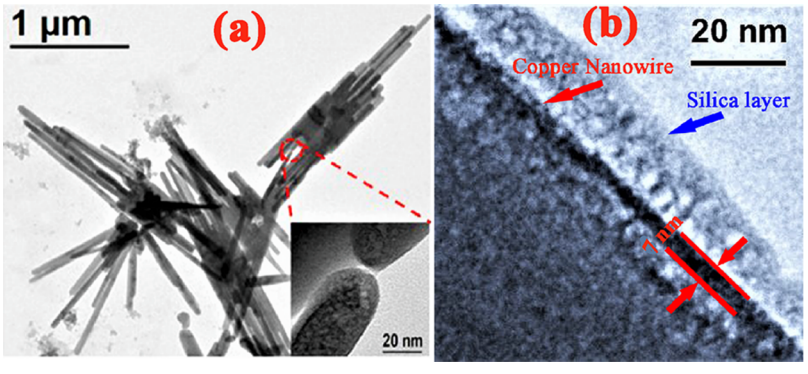

Figure 5. (a) TEM image of well-aligned copper nanowire obtained from thin film-1. Inset shows the disruption in nanowire. (b) HRTEM image of the copper nanowire with the silica layer obtained from thin film-1.

https://dx.doi.org/10.1021/acsomega.0c01186
ACS Omega 2020, 5, 12421−12430

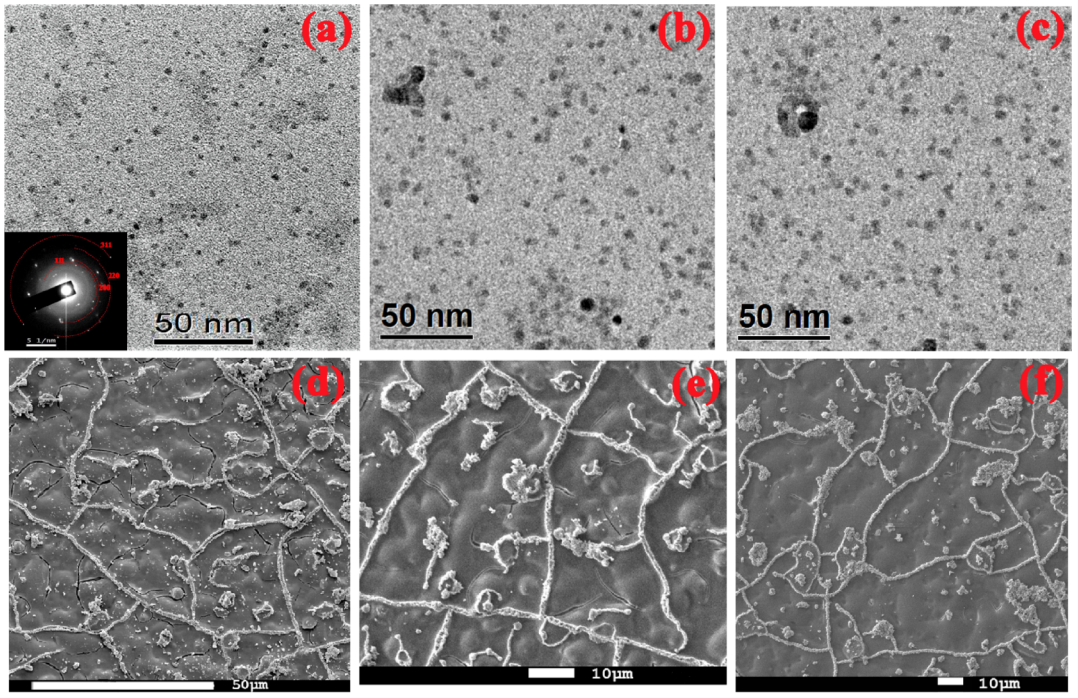

Figure 6. (a–c) TEM image showing the variation of the nanowire array density for 15, 30, and 45 min of deposition time for thin film-1. Inset of (a) shows the SAED pattern obtained from copper nanowire heads. (d–f) SEM image showing the variation of the nanowire length for 15, 30, and 45 min of deposition time for thin film-1.

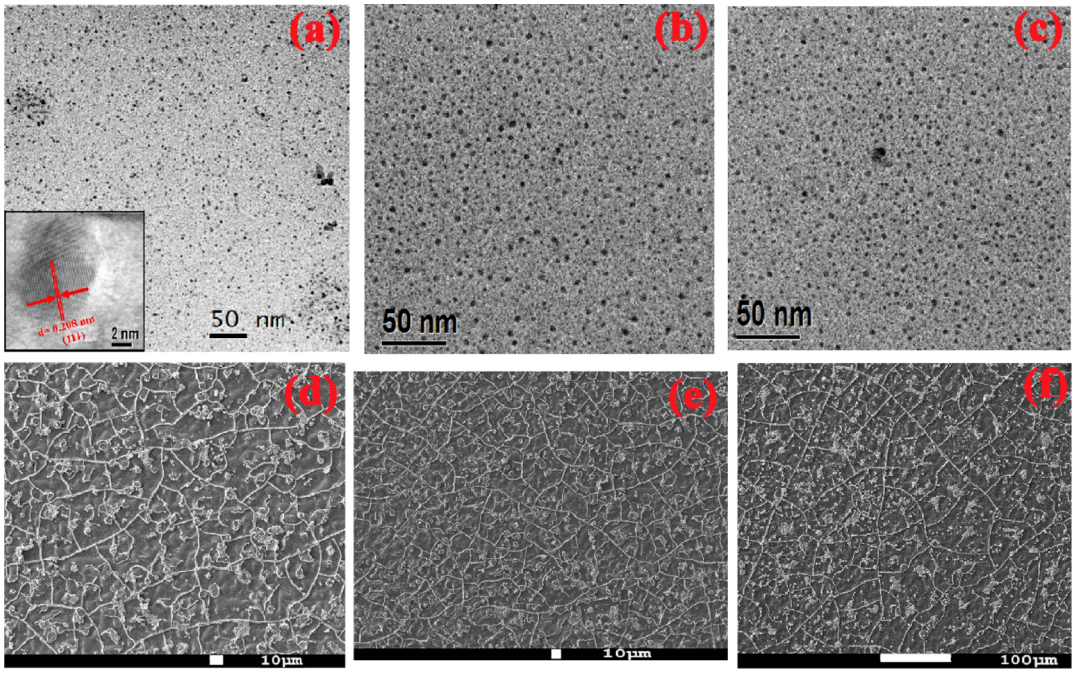

Figure 7. (a–c) TEM image showing the variation of the nanowire array density for 5, 10, and 15 min of deposition time for thin film-2. Inset of (a) shows the HRTEM of lattice planes obtained from copper nanowire heads. (d–f) SEM image showing the variation of the nanowire length for 5, 10, and 15 min of deposition time for thin film-2.

elemental and material analyses of our samples. Mapping by SEM provides qualitative information about the distribution of elements shown by different colors that were present in the scanned area. Figure 8a shows the area of thin film-2 containing copper nanowire subjected to elemental mapping, and the resulting EDS analysis is represented in Figure 8b. Figure 8c,e shows the relative positional stoichiometric occupancies of the constituent elements Cu, O, and Si.

The nonlinear current–voltage (I–V) data for the growth of the nanowires over a time period of 35 min within thin film-1 and thin film-2 are shown in Figure 9a,b. The electrochemical deposition process was performed by applying a dc voltage of 5 V magnitude across the electrodes for different time periods. It

https://dx.doi.org/10.1021/acsomega.0c01186
ACS Omega 2020, 5, 12421–12430

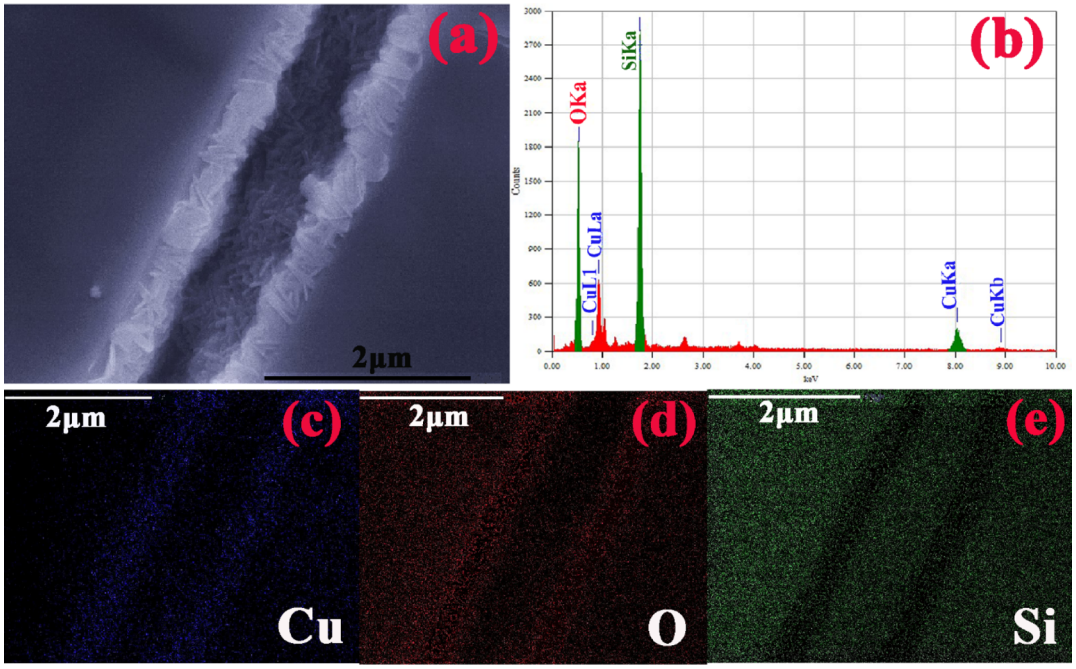

Figure 8. (a) Area of thin film-2 containing copper nanowire subjected to elemental mapping. (b) Resulting EDS analysis obtained from (a). (c–e) Relative positional stoichiometric occupancies of the constituent elements Cu, O, and Si obtained from (a).

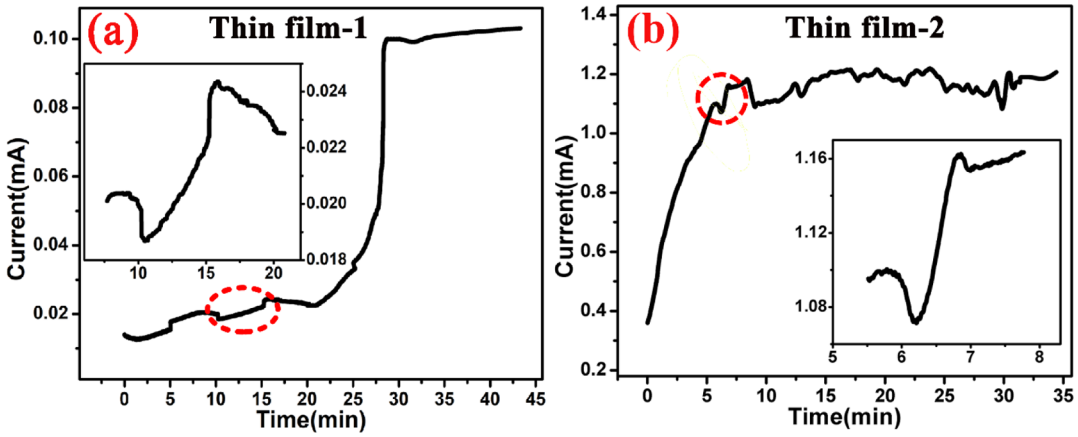

Figure 9. (a) *I*–*V* characteristic for thin film-1 during the electrodeposition process. Inset shows *I*–*V* characteristic at the point of nanowire disruption for thin film-1. (b) *I*–*V* characteristic for thin film-2 during the electrodeposition process. Inset shows *I*–*V* characteristic at the point of nanowire disruption for thin film-2.

is evident from this curve that as the time of electrodeposition was increased, the current through the sample also increased. Initially, the current increased very slowly for thin film-1 but attained a saturation value after 33 min, whereas in the case of thin film-2, time taken to reach the saturation value was 12 min which is much less than the earlier one. It may also be noted from the *I*–*V* data that the maximum current is reached for 15 min of deposition time for thin film-2, and with further longer deposition time (>15 min), the current does not change remarkably. Because of the smaller tip radius of the nanowire, the electric field strength intensifies which leads to the deposition of copper at the nanowire tip resulting in the increase of the nanowire length.[41] The further increment in the nanowire length is reflected by a sharp increase in current. The initial value and maximum magnitude of current flowing through the samples were found to be larger for thin film-2. The more available copper ions for thin film-2 made it easier for the competitive growth rates of metal Cu atoms entering the glass matrix and forming copper nanowires, as compared to thin film-1.[41,42] The Cu^{2+} ions drift toward the cathode under the influence of the applied electric field and get reduced to form the metallic copper crystal lattice. Initially, few nanowires started to grow when the available Cu^{2+} ions were reduced to form copper nanowires but as the easy availability of Cu^{2+} ions was reduced at the vicinity, its growth rate decreased[41] and then the other copper nanowires started to grow, thereby increasing the nanowire density over the electrodeposition time period.

Initially, few nanowires were disrupted at the weak junctions because of local heating effects. The high current density that may find only few paths (initially) to flow resulted in a sharp increase of temperature causing the nanowires to break at the weak junctions and disrupting the continuity of the nanowires. As and when one nanowire was disrupted, the other started to

https://dx.doi.org/10.1021/acsomega.0c01186
ACS Omega 2020, 5, 12421–12430

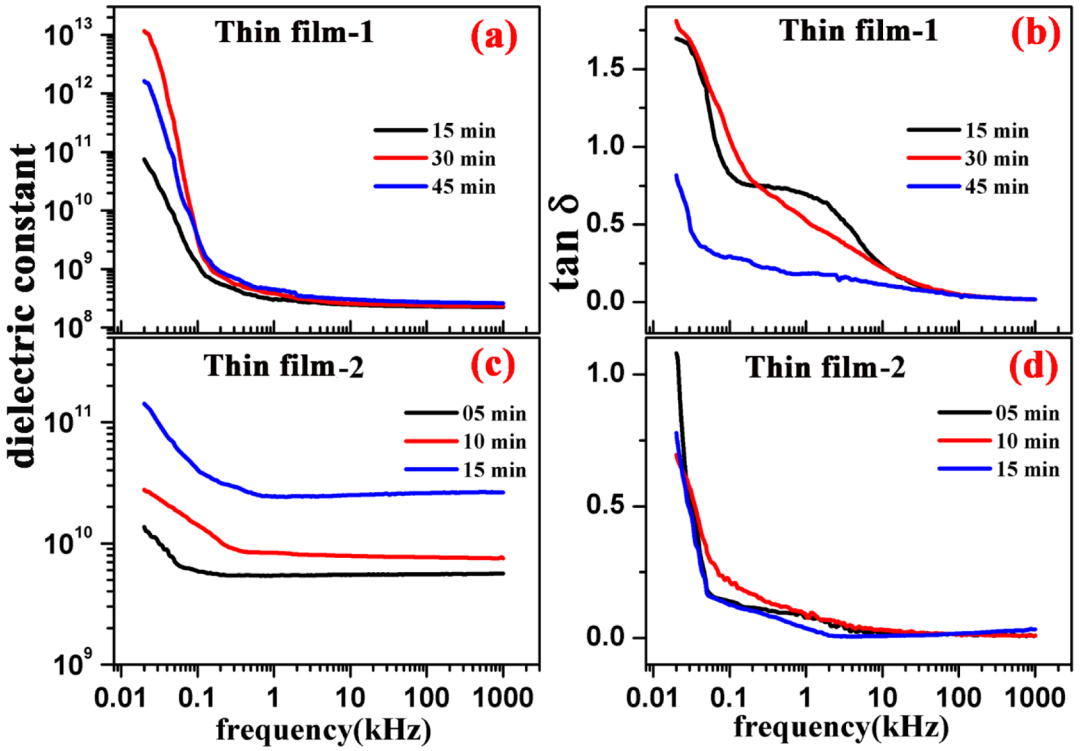

Figure 10. (a) Variation of dielectric constant as a function of frequency for thin film-1, (b) variation of dissipation factor as a function of frequency for thin film-1, (c) variation of dielectric constant as a function of frequency for thin film-2, and (d) variation of dissipation factor as a function of frequency for thin film-2.

form and the current through the sample increased. This is clearly shown in the inset of the TEM micrograph in Figure 5a. The process of disruption of the nanowires is also reflected in the $I-V$ curve; a sharp and sudden decrease of current is the signature of such a process. $I-V$ characteristics at the point of disruption are shown in the insets of Figure 9a,b.

Polarization of a dielectric material determines its energy storage ability. Among four kinds of dielectric polarization (orientational, interfacial, atomic, and electronic polarization), only atomic and electronic polarizations predominate at higher frequencies, whereas all others make their presence felt at lower frequencies.[43] Figure 10 shows the comparison between the variation of dielectric constant values and the dissipation factor (tan δ) measured at room temperature over the frequency range of 20 Hz to 1 MHz. It is evident from the figure that an asymptotic giant dielectric constant value of ~2.2 × 10^8 with a loss factor of 0.04 was obtained for thin film-1, whereas thin film-2 exhibited a dielectric constant value of ~2.5 × 10^{10} with a loss factor of ~0.01 at frequencies in the range 1 kHz−1 MHz. The details are presented in Table 1. The low dissipation factor is attributed to the masking of the copper nanowire with an insulating silica layer. Such high values of dielectric constant (~10^{10}) at high frequency with a low value of dissipation factor is reported for the first time to the best of our knowledge.

The dependence of dielectric constant of these materials as a function of frequency over the abovementioned frequency range (1 kHz−1 MHz) was very low, imparting a high-frequency stability of these materials. The displacement of negatively charged electron cloud from the positive charge center with the application of electric field gives rise to electronic polarization. By this research methodology, we have successfully designed nanowires having discrete electronic energy levels leading to enormously enhanced dielectric constant which was explained quantum mechanically by the Rice−Bernasconi model.[29] The quantum mechanical explanation of static dielectric constant of the metallic strand system is expressed as[29]

$$\varepsilon = \frac{1}{2}(q_s l_a)^2 \tag{1}$$

where ε is the static dielectric constant of the system, l_a is the average length of the metallic nanowire strands, and q_s is the Fermi−Thomas screening wave vector defined as follows

$$q_s^{\,2} = \frac{24 n_d e^2}{\hbar u_F} \tag{2}$$

where n_d is the nanowire array density per unit area perpendicular to the strand axis, and h, u_F, and e represent Plank's constant, electron velocity at the Fermi level, and electronic charge, respectively. Substituting the values of e, h, and u_F = 1.58 × 10^8 cm/s for copper[44] in eq 2, we get

$$q_s^{\,2} = 33.24\, n_d \tag{3}$$

Using the values of n_d and l_a, we have calculated the values of ε for different thin films which are summarized in Table 1. These results have been explained on the basis of the quantum mechanical effect of discrete electronic energy levels in a macroscopic system which are in good agreement with the experimentally obtained dielectric constant values for the two thin film samples studied here. This synthesis procedure and quantum mechanical explanation can be used to synthesize high-energy density materials with superior energy storage capacity.

https://dx.doi.org/10.1021/acsomega.0c01186
ACS Omega 2020, 5, 12421−12430

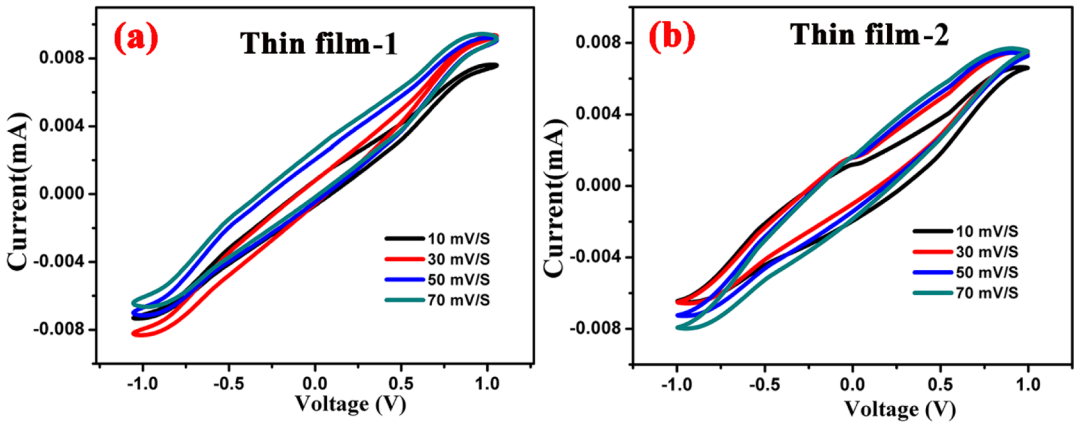

Figure 11. (a) CV curves for thin film-1 and (b) CV curves for thin film-2.

Electrochemical performance of the samples for supercapacitor applications was studied using a conventional two electrode system.[45] Figure 11a,b shows the CV curves of thin film-1 and thin film-2. The CV measurements were performed within the voltage range of −1 to +1 V at various scan rates. The specific capacitance value at different scan rates was obtained using the following equation[45]

$$C_v = \frac{\int_{E_2}^{E_1} I(E)\mathrm{d}E}{m_i k(E_1 - E_2)} \quad (4)$$

where m_1 = 0.35 mg and m_2 = 0.40 mg are the mass of the active material used for thin film-1 and thin film-2, respectively, k is the scan rate (V/s), and $\int_{E_2}^{E_1} I(E)\mathrm{d}E$ is the integrated area under the CV curve within the potential window E_2 and E_1 (i.e., −1 to +1 V) and summarized in Table 2. The maximum

Table 2. Comparative Data of Specific Capacitance for All the Samples

	specific capacitance (F/g)	
scan rate (mV/s)	thin film-1 (05 Cu_2O−95 SiO_2)	thin film-2 (15 Cu_2O−85 SiO_2)
10	249.28	550.00
20	132.86	241.43
50	102.71	109.71
70	86.12	92.86

specific capacitance of 550 F/g was obtained for thin film-2 at a scan rate of 10 mV/s within the investigated potential window. Although the scan rate varied over a wide range, the nature of the curve remained unaltered revealing a near ideal supercapacitor behavior with good rate capability.[46] The absence of any redox peak implies the ideal supercapacitor behavior between the copper nanowire and the residual electrolyte (Cu_2O−SiO_2). The increase in surface area of copper nanowires with the increase in nanowire density for thin film-2 rather than thin film-1 contributed to the higher specific capacitance values for these systems.[35,37]

Figure 12 shows the percentage capacitive retentivity as a function of cycle number for thin film-2. The material retains more than 73% of its initial capacitance even after 900 cycles measured at a scan rate of 50 mV/s. The negligible decrease in capacitance value even after 900 cycles indicates its long cycle

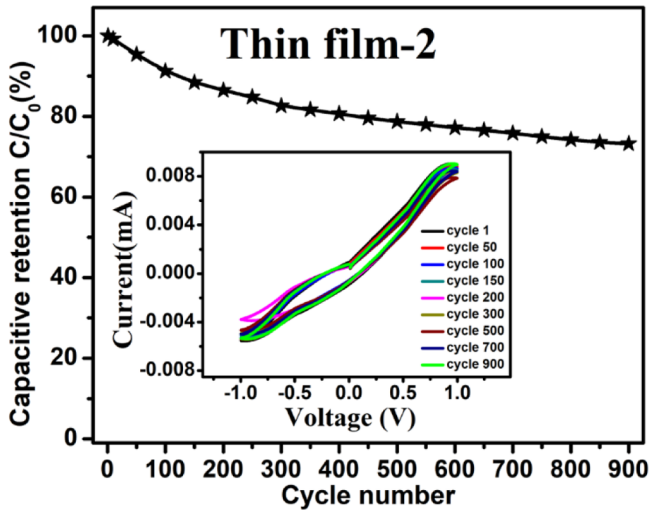

Figure 12. Percentage capacitive retentivity as a function of cycle number for thin film-2 measured at a scan rate of 50 mV/S. Inset shows the CV curves at different cycle numbers at a scan rate of 50 mV/S.

stability. Inset shows the CV curves at different cycle numbers at a scan rate of 50 mV/s for thin film-2.

We have carried out further nanostructure engineering of the metallic nanowire system with a higher concentration of the copper precursor (20 Cu_2O−80 SiO_2). We observed that there was no marked change in the investigated properties, except that the nanowires formed were thicker in diameter. It was also observed that the increase in the copper concentration scales down the transparency of the sample. Therefore, we have achieved an optimized supercapacitive performance for thin film-2.

CONCLUSIONS

Copper nanowires, having diameters in the range 7−9 nm and lengths in the range 52−387 μm, were synthesized within an amorphous silica matrix in the system Cu_2O/SiO_2 using a simple nonaqueous electrodeposition technique. These materials showed more than 80% transmittance over the optical wavelength range of 400−750 nm. The density of the nanowires was of the order of $(12-25)/(50 \times 50)$ nm^2. The nanowires grown were interrupted in their configuration. The composites exhibited very large values of dielectric constant of the order of 10^{10} in the high-frequency range. This was

https://dx.doi.org/10.1021/acsomega.0c01186
ACS Omega 2020, 5, 12421−12430

satisfactorily explained on the basis of the Rice−Bernasconi model of interrupted metallic nanowires. Electrochemical measurements revealed nearly ideal capacitive behavior expressing long cycle stability with a specific capacitance value of 550 F/g. Therefore, these materials may form the basis for fabricating transparent and stable thin film supercapacitors with potential application in energy storage devices.

AUTHOR INFORMATION

Corresponding Author

Dipankar Chakravorty − *School of Materials Science, Indian Association for the Cultivation of Science, Kolkata 700032, India;* orcid.org/0000-0002-4380-2594; Phone: +91-33-2473 4971 (ext 1580); Email: mlsdc@iacs.res.in; Fax: +91 33 2473 2805

Authors

Anupam Maity − *School of Materials Science, Indian Association for the Cultivation of Science, Kolkata 700032, India; Department of Physics, Jadavpur University, Kolkata 700032, India;* orcid.org/0000-0001-7572-6082

Subha Samanta − *School of Materials Science and School of Physical Science, Indian Association for the Cultivation of Science, Kolkata 700032, India;* orcid.org/0000-0002-6023-3493

Shubham Roy − *Department of Physics, Jadavpur University, Kolkata 700032, India;* orcid.org/0000-0001-5245-3229

Debasish Biswas − *Department of Physics, Jadavpur University, Kolkata 700032, India*

Complete contact information is available at: https://pubs.acs.org/10.1021/acsomega.0c01186

Notes

The authors declare no competing financial interest.

ACKNOWLEDGMENTS

A.M. acknowledges the award of NFSC, University Grants Commission, New Delhi. S.S. acknowledges the award of INSPIRE fellowship by Department of Science and Technology, New Delhi. D.C. thanks Indian National Science Academy, New Delhi for giving him an Emeritus Scientist position. We acknowledge the expert help of Arunim Paul of Indian Association for the Cultivation of Science, Kolkata in TEM characterization of all the samples.

REFERENCES

(1) Chen, P. C.; Shen, G.; Sukcharoenchoke, S.; Zhou, C. Flexible and Transparent Supercapacitor Based on In_2O_3 Nanowire/Carbon Nanotube Heterogeneous Films. *Appl. Phys. Lett.* **2009**, *94*, 043113.

(2) Zhang, D.; Wang, R.; Wen, M.; Weng, D.; Cui, X.; Sun, J.; Li, H.; Lu, Y. Synthesis of Ultralong Copper Nanowires for High-Performance Transparent Electrodes. *J. Am. Chem. Soc.* **2012**, *134*, 14283−14286.

(3) Tang, H.; Zhou, Z.; Sodano, H. A. Relationship between $BaTiO_3$ Nanowire Aspect Ratio and the Dielectric Permittivity of Nanocomposites. *ACS Appl. Mater. Interfaces* **2014**, *6*, 5450−5455.

(4) Tang, H.; Zhou, Z.; Bowland, C. C.; Sodano, H. A. Synthesis of Calcium Copper Titanate ($CaCu_3Ti_4O_{12}$) Nanowires with Insulating SiO_2 Barrier for Low Loss High Dielectric Constant Nanocomposites. *Nano Energy* **2015**, *17*, 302−307.

(5) Moitra, D.; Anand, C.; Ghosh, B. K.; Chandel, M.; Ghosh, N. N. One-Dimensional $BiFeO_3$ Nanowire-Reduced Graphene Oxide Nanocomposite as Excellent Supercapacitor Electrode Material. *ACS Appl. Energy Mater.* **2018**, *1*, 464−474.

(6) Zeraati, A. S.; Mirkhani, S. A.; Sundararaj, U. Enhanced Dielectric Performance of Polymer Nanocomposites Based on CNT/MnO_2 Nanowire Hybrid Nanostructure. *J. Phys. Chem. C* **2017**, *121*, 8327−8334.

(7) Yoon, Y. S.; Cho, W. I.; Lim, J. H.; Choi, D. J. Solid-State Thin-Film Supercapacitor with Ruthenium Oxide and Solid Electrolyte Thin Films. *J. Power Sources* **2001**, *101*, 126−129.

(8) Liu, C.; Yu, Z.; Neff, D.; Zhamu, A.; Jang, B. Z. Graphene-Based Supercapacitor with an Ultrahigh Energy Density. *Nano Lett.* **2010**, *10*, 4863−4868.

(9) Inamdar, A. I.; Kim, Y.; Pawar, S. M.; Kim, J. H.; Im, H.; Kim, H. Chemically Grown, Porous, Nickel Oxide Thin-Film for Electrochemical Supercapacitors. *J. Power Sources* **2011**, *196*, 2393−2397.

(10) Yu, W.; Jiang, X.; Ding, S.; Li, B. Q. Preparation and Electrochemical Characteristics of Porous Hollow Spheres of NiO Nanosheets as Electrodes of Supercapacitors. *J. Power Sources* **2014**, *256*, 440−448.

(11) Ji, J.; Zhang, L. L.; Ji, H.; Li, Y.; Zhao, X.; Bai, X.; Fan, X.; Zhang, F.; Ruoff, R. S. Nanoporous $Ni(OH)_2$ thin film on 3d Ultrathin-Graphite Foam for Asymmetric Supercapacitor. *ACS Nano* **2013**, *7*, 6237−6243.

(12) Liu, J.; Smith, R. W.; Mei, W.-N. Synthesis of the Giant Dielectric Constant Material $CaCu_3Ti_4O_{12}$ by Wet-Chemistry Methods. *Chem. Mater.* **2007**, *19*, 6020−6024.

(13) Homes, C. C. Optical Response of High-Dielectric-Constant Perovskite-Related Oxide. *Science* **2001**, *293*, 673−676.

(14) Mandal, B. P.; Anithakumari, P.; Nigam, S.; Majumder, C.; Mohapatra, M.; Tyagi, A. K. Enhancement of Dielectric Constant in a Niobium Doped Titania System: An Experimental and Theoretical Study. *New J. Chem.* **2016**, *40*, 9526−9536.

(15) Dang, Z.-M.; Zhou, T.; Yao, S.-H.; Yuan, J.-K.; Zha, J.-W.; Song, H.-T.; Li, J.-Y.; Chen, Q.; Yang, W.-T.; Bai, J. Advanced Calcium Copper Titanate/Polyimide Functional Hybrid Films with High Dielectric Permittivity. *Adv. Mater.* **2009**, *21*, 2077−2082.

(16) Chen, Y.; Fu, X.-Y.; Yue, Y.-Y.; Zhang, N.; Feng, J.; Sun, H.-B. Flexible and Transparent Supercapacitor Based on Ultrathin Au/Graphene Composite Electrodes. *Appl. Surf. Sci.* **2019**, *467−468*, 104−111.

(17) Maity, A.; Samanta, S.; Chatterjee, S.; Maiti, R.; Biswas, D.; Saha, S. K.; Chakravorty, D. Giant Dielectric Permittivity in Interrupted Silver Nanowires Grown within Mesoporous Silica. *J. Phys. D Appl. Phys.* **2018**, *51*, 245301.

(18) Samanta, S.; Maity, A.; Chatterjee, S.; Maiti, R.; Biswas, D.; Giri, S.; Chakravorty, D. Rice−Bernasconi Gorkov−Eliashberg Effect of Giant Dielectric Permittivity in Silica- Based Films Containing Interrupted Silver Nanowires. *Trans. Indian Inst. Met.* **2019**, *72*, 1963−1969.

(19) Wen, X.; Xie, Y.; Choi, C. L.; Wan, K. C.; Li, X.-Y.; Yang, S. Copper-Based Nanowire Materials: Templated Synthesis, Characterizations, and Applications. *Langmuir* **2005**, *21*, 4729−4737.

(20) Wang, N.; Fung, K. K.; Wang, S.; Yang, S. Oxide-Assisted Nucleation and Growth of Copper Sulphide Nanowire Arrays. *J. Cryst. Growth* **2001**, *233*, 226−232.

(21) Tokuda, N.; Watanabe, H.; Hojo, D.; Yamasaki, S.; Miki, K.; Yamabe, K. Fabrication of Cu Nanowires along Atomic Step Edge Lines on Si(1 1 1) Substrates. *Appl. Surf. Sci.* **2004**, *237*, 528−531.

(22) Liu, J.; Duan, C.-G.; Yin, W.-G.; Mei, W. N.; Smith, R. W.; Hardy, J. R. Large Dielectric Constant and Maxwell-Wagner Relaxation in $Bi_{2/3}Cu_3Ti_4O_{12}$. *Phys. Rev. B: Condens. Matter Mater. Phys.* **2004**, *70*, 144106.

(23) Li, W.; Schwartz, R. W. Maxwell-Wagner Relaxations and Their Contributions to the High Permittivity of Calcium Copper Titanate Ceramics. *Phys. Rev. B: Condens. Matter Mater. Phys.* **2007**, *75*, 012104.

(24) Lunkenheimer, P.; Fichtl, R.; Ebbinghaus, S. G.; Loidl, A. Nonintrinsic Origin of the Colossal Dielectric Constants in $CaCu_3Ti_4O_{12}$. *Phys. Rev. B: Condens. Matter Mater. Phys.* **2004**, *70*, 172102.

(25) Kubo, R. Electronic Properties of Metallic Fine Particles. I. *J. Phys. Soc. Jpn.* **1962**, *17*, 975−986.
(26) Gorkov, L. P.; Eliashberg, G. M. Minute Metallic Particles in an Electromagnetic Field. *Sov. Phys.—JETP* **1965**, *21*, 940.
(27) Dupree, R.; Smithard, M. a. The Electronic Properties of Small Metal Particles: The Electric Polarizability. *J. Phys. C Solid State Phys.* **1972**, *5*, 408−414.
(28) Strässler, S.; Rice, M. J.; Wyder, P. Comment on Gorkov and Eliashberg's Result for the Polarizability of a Minute Metallic Particle. *Phys. Rev. B: Condens. Matter Mater. Phys.* **1972**, *6*, 2575−2577.
(29) Rice, M. J.; Bernasconi, J. Gor'kov-Eliashberg Effect in One-Dimensional Metals? *Phys. Rev. Lett.* **1972**, *29*, 113−116.
(30) Ray, A.; Roy, A.; Bhattacharjee, S.; Jana, S.; Ghosh, C. K.; Sinha, C.; Das, S. Correlation between the Dielectric and Electrochemical Properties of TiO_2-V_2O_5 Nanocomposite for Energy Storage Application. *Electrochim. Acta* **2018**, *266*, 404−413.
(31) Lee, Y.-W.; Kim, B.-S.; Hong, J.; Lee, J.; Pak, S.; Jang, H.-S.; Whang, D.; Cha, S.; Sohn, J. I.; Kim, J. M. A Pseudo-Capacitive Chalcogenide-Based Electrode with Dense 1-Dimensional Nanoarrays for Enhanced Energy Density in Asymmetric Supercapacitors. *J. Mater. Chem. A* **2016**, *4*, 10084−10090.
(32) Hsu, Y.-K.; Chen, Y.-C.; Lin, Y.-G. Synthesis of Copper Sulfide Nanowire Arrays for High-Performance Supercapacitors. *Electrochim. Acta* **2014**, *139*, 401−407.
(33) Javed, M. S.; Dai, S.; Wang, M.; Xi, Y.; Lang, Q.; Guo, D.; Hu, C. Faradic Redox Active Material of Cu_7S_4 Nanowires with a High Conductance for Flexible Solid State Supercapacitors. *Nanoscale* **2015**, *7*, 13610−13618.
(34) Xu, P.; Ye, K.; Du, M.; Liu, J.; Cheng, K.; Yin, J.; Wang, G.; Cao, D. One-Step Synthesis of Copper Compounds on Copper Foil and Their Supercapacitive Performance. *RSC Adv.* **2015**, *5*, 36656−36664.
(35) Soam, A.; Kavle, P.; Kumbhar, A.; Dusane, R. O. Performance Enhancement of Micro- Supercapacitor by Coating of Graphene on Silicon Nanowires at Room Temperature. *Curr. Appl. Phys.* **2017**, *17*, 314−320.
(36) Devarayan, K.; Lei, D.; Kim, H.-Y.; Kim, B.-S. Flexible Transparent Electrode Based on PANi Nanowire/Nylon Nanofiber Reinforced Cellulose Acetate Thin film as Supercapacitor. *Chem. Eng. J.* **2015**, *273*, 603−609.
(37) Paravannoor, A.; Ranjusha, R.; Asha, A. M.; Vani, R.; Kalluri, S.; Subramanian, K. R. V.; Sivakumar, N.; Kim, T. N.; Nair, S. V.; Balakrishnan, A. Chemical and Structural Stability of Porous Thin film NiO Nanowire Based Electrodes for Supercapacitors. *Chem. Eng. J.* **2013**, *220*, 360−366.
(38) Maity, A.; Samanta, S.; Maiti, R.; Chatterjee, S.; Biswas, D.; Chakravorty, D. Giant Magnetodielectric Effect in Composites of Nanodimensional Spin Glass of System CoO- SiO_2 and Mesoporous Silica SBA-15. *J. Magn. Magn. Mater.* **2019**, *491*, 165633.
(39) Wei, Y.; Jin, D.; Ding, T.; Shih, W.-H.; Liu, X.; Cheng, S. Z. D.; Fu, Q. A Non-Surfactant Templating Route to Mesoporous Silica Materials. *Adv. Mater.* **1998**, *10*, 313−316.
(40) Mu, C.-H.; Liu, P.; He, Y.; Zhou, J.-P.; Zhang, H.-W. An Effective Method to Decrease Dielectric Loss of $CaCu_3Ti_4O_{12}$ Ceramics. *J. Alloys Compd.* **2009**, *471*, 137−141.
(41) Schmädicke, C.; Poetschke, M.; Renner, L. D.; Baraban, L.; Bobeth, M.; Cuniberti, G. Copper Nanowire Synthesis by Directed Electrochemical Nanowire Assembly. *RSC Adv.* **2014**, *4*, 46363−46368.
(42) Sawada, Y.; Dougherty, A.; Gollub, J. P. Dendritic and Fractal Patterns in Electrolytic Metal Deposits. *Phys. Rev. Lett.* **1986**, *56*, 1260−1263.
(43) Callister, W. D. J.; Rethswisch, D. G. *Materials Science and Engineering An Introduction*; John Wiley & Sons, Inc., 2014; p 990.
(44) Kittel, C. *Introduction to Solid State Physics*; John Wiley & Sons, Inc., 2005; p 455.
(45) Samanta, S.; Maity, A.; Chatterjee, S.; Giri, S.; Chakravorty, D. Composites of Nanodimensional Glass in the System Na_2O−SiO_2/Mesoporous Silica and Their High Ionic Conductivity. *J. Phys. Chem. Solids* **2020**, *142*, 109470.
(46) Cao, J.; Safdar, M.; Wang, Z.; He, J. High-Performance Flexible Supercapacitor Electrodes Based on Te Nanowire Arrays. *J. Mater. Chem. A* **2013**, *1*, 10024−10029.

https://dx.doi.org/10.1021/acsomega.0c01186
ACS Omega 2020, 5, 12421−12430